Paper
Int'l J. of Aeronautical & Space Sci. 16(2), 278–294 (2015)
DOI: http://dx.doi.org/10.5139/IJASS.2015.16.2.278

IJASS
International Journal of Aeronautical and Space Sciences

Integrated Guidance and Control Design for the Near Space Interceptor

WANG Fei* and LIU Gang**

Information Engineering College, Henan University of Science and Technology, Luoyang, China

LIANG Xiao-Geng***

Luoyang Optoelectro Technology Development Center, Luoyang, China

Abstract

Considering the guidance and control problem of the near space interceptor (NSI) during the terminal course, this paper proposes a three-channel independent integrated guidance and control (IGC) scheme based on the backstepping sliding mode and finite time disturbance observer (FTDO). Initially, the three-channel independent IGC model is constructed based on the interceptor-target relative motion and nonlinear dynamic model of the interceptor, in which the channel coupling term and external disturbance are regarded as the total disturbances of the corresponding channel. Then, the FTDO is introduced to estimate the target acceleration and control system loop disturbances, and the feed-forward compensation term based on the estimated values is employed to effectively remove the effect of disturbances in finite time. Subsequently, the IGC algorithm based on the backstepping sliding mode is also given to obtain the virtual control moment. Furthermore, a robust least-squares weighted control allocation (RLSWCA) algorithm is employed to distribute the previous virtual control moment among the corresponding aerodynamic fins and reaction jets, which also takes into account the uncertainty in the control effectiveness matrix. Finally, simulation results show that the proposed IGC method can obtain the small miss distance and smooth interceptor trajectories.

Key words: Integrated Guidance and Control (IGC), Finite Time Disturbance Observer (FTDO), Backstepping Sliding Mode, Robust Least-Squares weighted Control Allocation (RLSWCA)

1. Introduction

The guidance and control algorithm of the near space interceptor (NSI) is one of the most critical technologies to effectively deal with the threat of near space air-breathing hypersonic vehicles. The traditional design method is usually based on the assumption that the spectral separation between the guidance loop and control loop is satisfied, which may be invalid during the terminal interception phase [1]-[2]. Since this scheme cannot strictly guarantee the stability of the overall guidance and control system, the modifications of each subsystem are generally required to obtain overall system performance. By viewing the guidance and control loops as an integrated system and taking into account the coupling terms between these two subsystems, the integrated guidance and control (IGC) exploits the states of the interceptor and the interceptor-target motion to directly generate the actuator commands, which can efficiently reduce the cost of the required sensors and increase the guidance accuracy and system reliability [3]-[5].

The past few years have witnessed rapidly growing interest in the IGC design, and many approaches have been reported [6]-[13]. It is well known that sliding mode control is an effective technology to deal with system disturbance and parameter uncertainty. In [6] and [7], smooth second-order sliding mode (SSOSM) control is proposed to study the IGC design problem of the interceptor. The SSOSM-based guidance law is first developed to obtain the desired overload command, which can

* Associate Professor, Corresponding author: feiwangnpu@163.com
** Associate Professor
*** Professor

Received: December 29, 2014 Revised: June 13, 2015 Accepted: June 15, 2015

http://ijass.org pISSN: 2093-274x eISSN: 2093-2480

be transformed into the desired value of pitch angular rate in the inner loop. Subsequently, the SOSM-based control law is constructed to track the desired pitch angular rate in finite time and obtain the IGC algorithm. In fact, the methods in [6] and [7] belong to the partial IGC design, which still cannot break away from the constraint of the traditional separation design. A novel IGC design method based on the robust higher-order sliding mode is also given in [8]. Based on the principle of zeroing the line-of-sight (LOS) angular rate, the IGC design problem can be transformed into the stabilization of a third-order integral chain system. Furthermore, a global finite-time stabilization control law is proposed for the above system based on geometric homogeneity theory, and the compensation term based on the super twisting algorithm is given to obtain the strong robustness against the uncertainties caused by target maneuvers and interceptor aerodynamic parameter perturbation.

Some nonlinear optimal control methods have also been applied to the IGC design. For example, the state-dependent Riccati equation (SDRE) technique is introduced to solve the Hamilton-Jacobi-Bellman (HJB) equation online in the nonlinear optimal control for the IGC design [9], but it is time consuming. Furthermore, the θ-D method is used to approximately solve the HJB equation, which did not require the online numerical computation [10]. Furthermore, the methods in [9] and [10] cannot ensure the robustness of the closed-loop system in the presence of system disturbances and parameter uncertainties. In [11], a novel IGC design approach based on the small-gain theorem and input-to-state stability (ISS) theory is proposed for missiles steered by both canard and tail controls without the assumption that the angle between LOS and missile velocity is almost constant. Theoretical analysis shows that both the LOS angular rate and the tracking error of the attitude angle (rate) are practically stable with respect to target maneuvers and missile model uncertainties. However, most of the above design methods [6]-[13] have not considered the uncertainties and disturbances or dealt with the effect of system disturbances at the price of sacrificing the normal control performance.

On the other hand, disturbance observer-based control (DOBC) provides an active approach to deal with system disturbances and uncertainties (see e.g., [14]-[16] and the references therein for a survey of recent development), and has been successfully applied in many fields, such as missiles [17]-[18] and hypersonic vehicle [19]. In order to completely remove the effect of system disturbances in finite time, finite time disturbance observer (FTDO) has also drawn much attention in the past few years [20]. Due to the redundancy of the NSI actuators (aerodynamic fins and reaction jets), control allocation is an effective scheme to distribute the virtual control command among the individual actuators [21]. Therefore, a novel robust least-squares weighted control allocation (RLSWCA) algorithm is proposed to deal with the above control allocation problem while taking into account the uncertainties in the control effectiveness matrix and the uneven distribution problem of the NSI actuator inputs [22]-[23].

Motivated by the above analysis, we will study the three-channel independent IGC design problem for the NSI based on the backstepping sliding mode and FTDO. By viewing the channel coupling term and external disturbance as the total disturbances of the corresponding channel, a three-channel independent IGC model is given for the NSI. Then, the FTDO is introduced to estimate the target acceleration and control system loop disturbances, and the backstepping sliding mode control law based on the estimated value is given to obtain the virtual control moment, in which the first-order low-pass filters are introduced to compute the differentiations of the virtual control variables at each step of the backstepping control. Furthermore, the RLSWCA algorithm is employed to distribute the previously virtual control moment among the corresponding actuators. Finally, simulation results show the effectiveness of the proposed design method.

Briefly, the rest of this paper is organized as follows. Section 2 introduces the three-channel independent IGC model for the NSI. Section 3 presents the corresponding IGC design method and RLSWCA algorithm. Section 4 gives the simulation results for the NSI guidance and control system. Finally, a brief conclusion is drawn in Section 5.

2. IGC model description

The interceptor-target motion in the three-dimensional space can be seen in Fig. 1, and the kinematical equations are described as follows [24]:

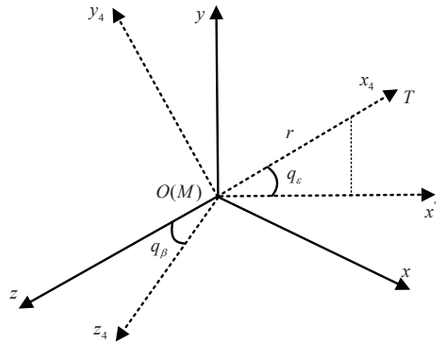

Fig. 1. Interceptor-target motion in three-dimensional space

$$\ddot{r} - r\dot{q}_\varepsilon^2 - r\dot{q}_\beta^2 \cos^2 q_\varepsilon = a_{tr} - a_{m4r} \tag{1}$$

$$r\ddot{q}_\varepsilon + 2\dot{r}\dot{q}_\varepsilon + r\dot{q}_\beta^2 \sin q_\varepsilon \cos q_\varepsilon = a_{t\varepsilon} - a_{m4\varepsilon} \tag{2}$$

$$-r\ddot{q}_\beta \cos q_\varepsilon - 2\dot{r}\dot{q}_\beta \cos q_\varepsilon + 2r\dot{q}_\varepsilon \dot{q}_\beta \sin q_\varepsilon = a_{t\beta} - a_{m4\beta} \tag{3}$$

where r is the relative distance between the interceptor and target, q_ε and q_β are the azimuth angle and elevation angle in the LOS coordinate system, $[a_{m4r}, a_{m4\varepsilon}, a_{m4\beta}]^T$ and $[a_{tr}, a_{t\varepsilon}, a_{t\beta}]^T$ are the interceptor and target accelerations in the LOS coordinate system, respectively.

The dynamic equations of the NSI in the three independent channels (pitch, yaw and roll) can be written as follows:

$$\begin{cases} \dot{\alpha} = \omega_z - \dfrac{qSC_y^\alpha \alpha}{mV_m} + \omega_y \tan\beta \sin\alpha - \omega_x \tan\beta \cos\alpha + d_\alpha \\ \dot{\omega}_z = \dfrac{qS\bar{L}m_z^\alpha \alpha}{J_z} + \dfrac{qS\bar{L}m_z^{\omega_z}\omega_z}{J_z} + \dfrac{M_z}{J_z} + \dfrac{J_x - J_y}{J_z}\omega_x\omega_y + d_{\omega_z} \\ a_{m3\varepsilon} = \dfrac{qSC_y^\alpha \alpha}{mg} \end{cases} \tag{4}$$

$$\begin{cases} \dot{\beta} = \omega_y + \dfrac{qSC_z^\beta \beta}{mV_m} + \omega_x \sin\alpha + \dfrac{qSC_y^\alpha \alpha \sin\alpha \sin\beta}{mV_m} + d_\beta \\ \dot{\omega}_y = \dfrac{qS\bar{L}m_y^\beta \beta}{J_y} + \dfrac{qS\bar{L}m_y^{\omega_y}\omega_y}{J_y} + \dfrac{M_y}{J_y} + \dfrac{J_z - J_x}{J_y}\omega_x\omega_z + d_{\omega_y} \\ a_{m3\beta} = \dfrac{qSC_z^\beta \beta}{mg} \end{cases} \tag{5}$$

$$\begin{cases} \dot{\gamma} = \omega_x - \omega_y \cos\gamma \tan\vartheta + \omega_z \sin\gamma \tan\vartheta + d_\gamma \\ \dot{\omega}_x = \dfrac{M_x}{J_x} + \dfrac{J_y - J_z}{J_x}\omega_y\omega_z + d_{\omega_x} \end{cases} \tag{6}$$

where q is the dynamic pressure; α, β and γ are the angle of attack, sideslip angle and roll angle; C_y^α, m_z^α, $m_z^{\omega_z}$, C_z^β, m_y^β and $m_y^{\omega_y}$ are the corresponding aerodynamic coefficients; d_α, d_{ω_z}, d_β, d_{ω_y}, d_γ and d_{ω_x} are the external disturbances; $a_{m3\varepsilon}$ and $a_{m3\beta}$ are the interceptor accelerations in the velocity coordinate system, respectively; M_z, M_y and M_x are the moments in the pitch, yaw and roll directions, which are mainly produced by the aerodynamic fins and reaction jet devices. It is also assumed that the lateral thrusts produced by the reaction jet devices are treated as the continuous variables [25]. Then, define the following equivalent control surface deflections of the lateral thrusts in the pitch and yaw directions [25]:

$$\delta_{sy} = F_y / F_{s\max}, \quad \delta_{sz} = F_z / F_{s\max} \tag{7}$$

where F_y and F_z denote the lateral thrusts in the pitch and yaw directions, $F_{s\max}$ is the maximum steady thrust of the reaction jets.

Define the following virtual control moment:

$$\boldsymbol{v} = (\boldsymbol{B}_c + \Delta\boldsymbol{B}_c)\boldsymbol{u} \tag{8}$$

where $\Delta\boldsymbol{B}_c$ is the uncertainty in the control effectiveness matrix, and

$$\boldsymbol{v} = [\bar{v}_r, \bar{v}_y, \bar{v}_p]^T = [M_x, M_y, M_z]^T,$$

$$\boldsymbol{u} = [\delta_x, \delta_y, \delta_z, \delta_{sy}, \delta_{sz}]^T, \quad \boldsymbol{B}_c = [\boldsymbol{B}_{c1}, \boldsymbol{B}_{c2}],$$

$$\boldsymbol{B}_{c1} = \begin{bmatrix} qS\bar{L}m_x^{\delta_x} & 0 & 0 \\ 0 & qS\bar{L}m_y^{\delta_y} & 0 \\ 0 & 0 & qS\bar{L}m_z^{\delta_z} \end{bmatrix},$$

$$\boldsymbol{B}_{c2} = \begin{bmatrix} 0 & 0 \\ 0 & (1+K_{M_y})F_{s\max}L_m \\ (1+K_{M_z})F_{s\max}L_m & 0 \end{bmatrix}.$$

It is assumed that the angles between LOS and the interceptor velocity coordinate system are small [1], i.e., $a_{m4\varepsilon} \approx a_{m3\varepsilon}$ and $a_{m4\beta} \approx a_{m3\beta}$. Based on equations (1)~(6), we can obtain the IGC model in the pitch channel:

$$\begin{cases} \dot{x}_{p2} = a_{p22}x_{p2} + a_{p23}x_{p3} - x_{y2}^2 \sin x_{p1} \cos x_{p1} + \dfrac{a_{t\varepsilon}}{r} \\ \dot{x}_{p3} = a_{p33}x_{p3} + x_{p4} + d_{p3} \\ \dot{x}_{p4} = a_{p43}x_{p3} + a_{p44}x_{p4} + b_{p4}\bar{v}_p + d_{p4} \\ y_{p2} = x_{p2} \end{cases} \tag{9}$$

where

$$x_{p1} = q_\varepsilon, \quad x_{p2} = \dot{q}_\varepsilon, \quad x_{p3} = \alpha, \quad x_{p4} = \omega_z, \quad \bar{v}_p = M_z,$$

$$a_{p22} = -\frac{2\dot{r}}{r}, \quad a_{p23} = -\frac{qSC_y^\alpha}{mr}, \quad a_{p33} = -\frac{qSC_y^\alpha}{mV_m}, \quad a_{p43} = \frac{qS\bar{L}m_z^\alpha}{J_z},$$

$$a_{p44} = \frac{qS\bar{L}m_z^{\omega_z}}{J_z}, \quad b_{p4} = \frac{1}{J_z},$$

$$d_{p3} = \omega_y \tan\beta \sin\alpha - \omega_x \tan\beta \cos\alpha + d_\alpha,$$

$$d_{p4} = \frac{J_x - J_y}{J_z}\omega_x\omega_y + d_{\omega_z};$$

the IGC model in the yaw channel:

$$\begin{cases} \dot{x}_{y2} = a_{y22}x_{y2} + a_{y23}x_{y3} + 2x_{p2}x_{y2} \tan x_{p1} - \dfrac{a_{t\beta}}{r\cos x_{p1}} \\ \dot{x}_{y3} = a_{y33}x_{y3} + x_{y4} + d_{y3} \\ \dot{x}_{y4} = a_{y43}x_{y3} + a_{y44}x_{y4} + b_{y4}\bar{v}_y + d_{y4} \\ y_{y2} = x_{y2} \end{cases} \tag{10}$$

DOI: http://dx.doi.org/10.5139/IJASS.2015.16.2.278

where

$$x_{y1}=q_\beta,\ x_{y2}=\dot{q}_\beta,\ x_{y3}=\beta,\ x_{y4}=\omega_y,\ \overline{v}_y=M_y,$$

$$a_{y22}=-\frac{2\dot{r}}{r},\ a_{y23}=\frac{qSC_z^\beta}{mr\cos x_{p1}},\ a_{y33}=\frac{qSC_z^\beta}{mV_m},\ a_{y43}=\frac{qS\overline{L}m_y^\beta}{J_y},$$

$$a_{y44}=\frac{qS\overline{L}m_y^{\omega_y}}{J_y},\ b_{y4}=\frac{1}{J_y},\ d_{y3}=\omega_x\sin\alpha+\frac{qSC_y^\alpha\alpha\sin\alpha\sin\beta}{mV_m}+d_\beta,$$

$$d_{y4}=\frac{J_z-J_x}{J_y}\omega_x\omega_z+d_{\omega_y};$$

and the IGC model in the roll channel:

$$\begin{cases}\dot{x}_{r3}=x_{r4}+d_{r3}\\ \dot{x}_{r4}=b_{r4}\overline{v}_r+d_{r4}\end{cases}\tag{11}$$

where

$$x_{r3}=\gamma,\ x_{r4}=\omega_x,\ \overline{v}_r=M_x,$$

$$d_{r3}=-\omega_y\cos\gamma\tan\vartheta+\omega_z\sin\gamma\tan\vartheta+d_\gamma,$$

$$b_{r4}=\frac{1}{J_x},\ d_{r4}=\frac{J_y-J_z}{J_x}\omega_y\omega_z+d_{\omega_x}.$$

Therefore, the IGC design objective is to derive the LOS angular rate from zero so that it is as small as possible, and guarantee the stability of the NSI dynamic simultaneously — i.e., the design an appropriate controller for the time-varying systems (9)~(11) to make the absolute values of the outputs as small as possible.

3. IGC design and stability analysis

In this section, a novel IGC algorithm is developed for the time-varying systems (9)~(11) based on the backstepping sliding mode and FTDO, and the stability analysis is also given for the closed-loop IGC system.

3.1 Control design in the pitch channel

Define the variable $v_\varepsilon=r\dot{q}_\varepsilon$, and based on equations (2) and (9), we can obtain:

$$\dot{v}_\varepsilon=-\frac{v_r v_\varepsilon}{r}-\frac{v_\beta^2\tan x_{p1}}{r}-\frac{qSC_y^\alpha}{m}x_{p3}+a_{t\varepsilon}\tag{12}$$

Then, the following FTDO is proposed to estimate the target acceleration :

$$\begin{cases}\dot{z}_{p20}=v_{p20}+f_{p2},\dot{z}_{p21}=v_{p21},\dot{z}_{p22}=v_{p22}\\ v_{p20}=-\lambda_{p20}L_{p2}^{1/3}|z_{p20}-v_\varepsilon|^{2/3}\mathrm{sgn}(z_{p20}-v_\varepsilon)+z_{p21}\\ v_{p21}=-\lambda_{p21}L_{p2}^{1/2}|z_{p21}-v_{p20}|^{1/2}\mathrm{sgn}(z_{p21}-v_{p20})+z_{p22}\\ v_{p22}=-\lambda_{p22}L_{p2}|z_{p22}-v_{p21}|^{q_{p2}/p_{p2}}\mathrm{sgn}(z_{p22}-v_{p21})\\ z_{p20}=\hat{v}_\varepsilon,z_{p21}=\hat{a}_{t\varepsilon},z_{p22}=\hat{\dot{a}}_{t\varepsilon}\end{cases}\tag{13}$$

where $f_{p2}=-\frac{v_r v_\varepsilon}{r}-\frac{v_\beta^2\tan x_{p1}}{r}-\frac{qSC_y^\alpha}{m}x_{p3}$, $\hat{v}_\varepsilon$ and $\hat{a}_{t\varepsilon}$ are the estimated values of v_ε and $a_{t\varepsilon}$, respectively; λ_{p20}, λ_{p21} and λ_{p22} are the observer gain coefficients to be determined.

When we define the error variables $e_{p20}=z_{p20}-v_\varepsilon$, $e_{p21}=z_{p21}-a_{t\varepsilon}$ and $e_{p22}=z_{p22}-\dot{a}_{t\varepsilon}$, we can obtain the following error system:

$$\begin{cases}\dot{e}_{p20}=-\lambda_{p20}L_{p2}^{1/3}|e_{p20}|^{2/3}\mathrm{sgn}(e_{p20})+e_{p21}\\ \dot{e}_{p21}=-\lambda_{p21}L_{p2}^{1/2}|e_{p21}-\dot{e}_{p20}|^{1/2}\mathrm{sgn}(e_{p21}-\dot{e}_{p20})+e_{p22}\\ \dot{e}_{p22}=-\lambda_{p22}L_{p2}|e_{p22}-\dot{e}_{p21}|^{q_{p2}/p_{p2}}\mathrm{sgn}(e_{p22}-\dot{e}_{p21})-\ddot{a}_{t\varepsilon}\end{cases}\tag{14}$$

Based on reference [20], we can determine that the error system (14) is stable in terms of finite time. Then, the following FTDOs are also introduced to estimate the disturbances d_{p3} and d_{p4} in the angle of the attack loop and pitch angular rate loop:

$$\begin{cases}\dot{z}_{p30}=v_{p30}+f_{p3},\dot{z}_{p31}=v_{p31},\dot{z}_{p32}=v_{p32}\\ v_{p30}=-\lambda_{p30}L_{p3}^{1/3}|z_{p30}-x_{p3}|^{2/3}\mathrm{sgn}(z_{p30}-x_{p3})+z_{p31}\\ v_{p31}=-\lambda_{p31}L_{p3}^{1/2}|z_{p31}-v_{p30}|^{1/2}\mathrm{sgn}(z_{p31}-v_{p30})+z_{p32}\\ v_{p32}=-\lambda_{p32}L_{p3}|z_{p32}-v_{p31}|^{q_{p3}/p_{p3}}\mathrm{sgn}(z_{p32}-v_{p31})\\ z_{p30}=\hat{x}_{p3},z_{p31}=\hat{d}_{p3},z_{p32}=\hat{\dot{d}}_{p3}\end{cases}\tag{15}$$

$$\begin{cases}\dot{z}_{p40}=v_{p40}+f_{p4},\dot{z}_{p41}=v_{p41},\dot{z}_{p42}=v_{p42}\\ v_{p40}=-\lambda_{p40}L_{p4}^{1/3}|z_{p40}-x_{p4}|^{2/3}\mathrm{sgn}(z_{p40}-x_{p4})+z_{p41}\\ v_{p41}=-\lambda_{p41}L_{p4}^{1/2}|z_{p41}-v_{p40}|^{1/2}\mathrm{sgn}(z_{p41}-v_{p40})+z_{p42}\\ v_{p42}=-\lambda_{p42}L_{p4}|z_{p42}-v_{p41}|^{q_{p4}/p_{p4}}\mathrm{sgn}(z_{p42}-v_{p41})\\ z_{p40}=\hat{x}_{p4},z_{p41}=\hat{d}_{p4},z_{p42}=\hat{\dot{d}}_{p4}\end{cases}\tag{16}$$

where $f_{p3}=a_{p33}x_{p3}+x_{p4}$, $f_{p4}=a_{p43}x_{p3}+a_{p44}x_{p4}+b_{p4}\overline{v}_p$, $\hat{d}_{p3}$ and $\hat{d}_{p4}$ are the estimated values of the disturbances d_{p3} and d_{p4}, respectively; the corresponding disturbance estimated errors are defined as $e_{p31}=z_{p31}-d_{p3}$ and $e_{p41}=z_{p41}-d_{p4}$.

Based on the FTDOs (13) and (15)~(16), the following backstepping sliding mode control law is given for the IGC system (9):

Step 1: Define the first error surface as follows:

$$s_{p2} = -a_{p23}^{-1}(x_{p2} - x_{p2d}) \tag{17}$$

where x_{p2d} is the command signal for the system (9), and the derivative of s_{p2} is:

$$\dot{s}_{p2} = a_{p23}^{-2}\dot{a}_{p23}(x_{p2} - x_{p2d}) - a_{p23}^{-1}(a_{p22}x_{p2} - x_{y2}^2 \sin x_{p1} \cos x_{p1} + a_{t\varepsilon} / r - \dot{x}_{p2d}) - x_{p3} \tag{18}$$

Then, the virtual control x_{p3}^* is constructed as follows:

$$x_{p3}^* = a_{p23}^{-2}\dot{a}_{p23}(x_{p2} - x_{p2d}) - a_{p23}^{-1}(a_{p22}x_{p2} - x_{y2}^2 \sin x_{p1} \cos x_{p1} + \hat{a}_{t\varepsilon} / r - \dot{x}_{p2d}) + k_{p2}s_{p2} \tag{19}$$

where $k_{p2}>0$. In addition, the following first-order low-pass filter is introduced to obtain the filtered virtual control $\bar{x}_{p3}^*$:

$$\tau_{p3}\dot{\bar{x}}_{p3}^* + \bar{x}_{p3}^* = x_{p3}^*, \quad \bar{x}_{p3}^*(0) = x_{p3}^*(0) \tag{20}$$

where $\tau_{p3}>0$ denotes the filter time constant. Then, we can obtain the differentiation of the filtered virtual control:

$$\dot{\bar{x}}_{p3}^* = -\tau_{p3}^{-1}(\bar{x}_{p3}^* - x_{p3}^*) \tag{21}$$

Step 2: Denote the second error surface as follows:

$$s_{p3} = x_{p3} - \bar{x}_{p3}^* \tag{22}$$

and its derivative is:

$$\dot{s}_{p3} = a_{p33}x_{p3} + x_{p4} + d_{p3} - \dot{\bar{x}}_{p3}^* \tag{23}$$

Then, the virtual control x_{p4}^* is constructed as follows:

$$x_{p4}^* = -a_{p33}x_{p3} - \hat{d}_{p3} + \dot{\bar{x}}_{p3}^* - k_{p3}s_{p3} \tag{24}$$

where $k_{p3}>0$. In addition, the following first-order low-pass filter is proposed to obtain the filtered virtual control $\bar{x}_{p4}^*$:

$$\tau_{p4}\dot{\bar{x}}_{p4}^* + \bar{x}_{p4}^* = x_{p4}^*, \quad \bar{x}_{p4}^*(0) = x_{p4}^*(0) \tag{25}$$

where $\tau_{p4}>0$ denotes the filter time constant. Then, we can obtain the differentiation of the filtered virtual control:

$$\dot{\bar{x}}_{p4}^* = -\tau_{p4}^{-1}(\bar{x}_{p4}^* - x_{p4}^*) \tag{26}$$

Step 3: Denote the third error surface as follows:

$$s_{p4} = x_{p4} - \bar{x}_{p4}^* \tag{27}$$

and its derivative is:

$$\dot{s}_{p4} = a_{p43}x_{p3} + a_{p44}x_{p4} + b_{p4}\bar{v}_p + d_{p4} - \dot{\bar{x}}_{p4}^* \tag{28}$$

Then, we can construct the following control moment:

$$\bar{v}_p = b_{p4}^{-1}[-a_{p43}x_{p3} - a_{p44}x_{p4} - \hat{d}_{p4} + \dot{\bar{x}}_{p4}^* - k_{p4}s_{p4} - k_{p5}|s_{p4}|^{\lambda_{p4}} \operatorname{sgn}(s_{p4})] \tag{29}$$

where $k_{p4}>0$, $k_{p5}>0$ and $0<\lambda_{p4}>0<1$.

3.2 Control design in the yaw channel

Define the variable $v_\beta = r\dot{q}_\beta \cos q_\varepsilon$, and based on equations (3) and (10), we can obtain:

$$\dot{v}_\beta = -\frac{v_r v_\beta}{r} + \frac{v_\varepsilon v_\beta \tan x_{p1}}{r} + \frac{qSC_z^\beta}{m}x_{y3} - a_{t\beta} \tag{30}$$

Then, the following FTDO is proposed to estimate the target acceleration $a_{t\beta}$:

$$\begin{cases} \dot{z}_{y20} = v_{y20} + f_{y2}, \dot{z}_{y21} = v_{y21}, \dot{z}_{y22} = v_{y22} \\ v_{y20} = -\lambda_{y20}L_{y2}^{1/3}|z_{y20} - v_\beta|^{2/3}\operatorname{sgn}(z_{y20} - v_\beta) + z_{y21} \\ v_{y21} = -\lambda_{y21}L_{y2}^{1/2}|z_{y21} - v_{y20}|^{1/2}\operatorname{sgn}(z_{y21} - v_{y20}) + z_{y22} \\ v_{y22} = -\lambda_{y22}L_{y2}|z_{y22} - v_{y21}|^{q_{y2}/p_{y2}}\operatorname{sgn}(z_{y22} - v_{y21}) \\ z_{y20} = \hat{v}_\beta, z_{y21} = -\hat{a}_{t\beta}, z_{y22} = -\dot{\hat{a}}_{t\beta} \end{cases} \tag{31}$$

where $f_{y2} = -\frac{v_r v_\beta}{r} + \frac{v_\varepsilon v_\beta \tan x_{p1}}{r} + \frac{qSC_z^\beta}{m}x_{y3}$, z_{y21} is the estimated value of target acceleration $-a_{t\beta}$, and the estimated error is defined as $e_{y21}=-z_{y21}-a_{t\beta}$. The similar FTDOs are also constructed to estimate the disturbances d_{y3} and d_{y4} in the sideslip angle loop and yaw angular rate loop, and the estimated errors are defined as $e_{y31}=-z_{y31}-d_{y3}$ and $e_{y41}=-z_{y41}-d_{y4}$.

Furthermore, we consider the following backstepping sliding mode control law for the system (10):

$$\begin{cases} s_{y2} = -a_{y23}^{-1}(x_{y2} - x_{y2d}) \\ x_{y3}^* = a_{y23}^{-2}\dot{a}_{y23}(x_{y2} - x_{y2d}) + k_{y2}s_{y2} \\ \qquad - a_{y23}^{-1}\left(a_{y22}x_{y2} + 2x_{p2}x_{y2}\tan x_{p1} - \frac{\hat{a}_{t\beta}}{r\cos x_{p1}} - \dot{x}_{y2d}\right) \\ \tau_{y3}\dot{\bar{x}}_{y3}^* + \bar{x}_{y3}^* = x_{y3}^*, \bar{x}_{y3}^*(0) = x_{y3}^*(0) \\ s_{y3} = x_{y3} - \bar{x}_{y3}^* \\ x_{y4}^* = -a_{y33}x_{y3} - \hat{d}_{y3} + \dot{\bar{x}}_{y3}^* - k_{y3}s_{y3} \\ \tau_{y4}\dot{\bar{x}}_{y4}^* + \bar{x}_{y4}^* = x_{y4}^*, \bar{x}_{y4}^*(0) = x_{y4}^*(0) \\ s_{y4} = x_{y4} - \bar{x}_{y4}^* \\ \bar{v}_y = b_{y4}^{-1}[-a_{y43}x_{y3} - a_{y44}x_{y4} - \hat{d}_{y4} + \dot{\bar{x}}_{y4}^* - k_{y4}s_{y4} - k_{y5}|s_{y4}|^{\lambda_{y4}}\operatorname{sgn}(s_{y4})] \end{cases} \tag{32}$$

where $0<\lambda_{y4}<1$; s_{y2}, s_{y3} and s_{y4} are the error surfaces of the guidance loop, sideslip angle loop and yaw angular rate loop in the yaw channel; k_{y2}, k_{y3} and k_{y4} are the corresponding error surface gains; τ_{y3} and τ_{y4} are the filter time constants; x_{y3}^* and x_{y4}^* are the virtual control of the guidance loop and sideslip angle loop in the yaw channel; $\bar{x}_{y3}^*$ and $\bar{x}_{y4}^*$ are the corresponding filtered virtual control.

3.3 Control design in the roll channel

In this section, we firstly design the FTDOs to estimate the

disturbances d_{r3} and d_{r4} in the roll angle loop and roll angular rate loop, and the estimated errors are defined as $e_{r31}=z_{r31}-d_{r3}$ and $e_{r41}=z_{r41}-d_{r4}$, respectively.

For the system (11), we consider the similar backstepping sliding mode control law:

$$\begin{cases} s_{r3} = x_{r3} - x_{r3d} \\ x_{r4}^* = -\hat{d}_{r3} + \dot{x}_{r3d} - k_{r3}s_{r3} \\ \tau_{r4}\ddot{\bar{x}}_{r4}^* + \dot{\bar{x}}_{r4}^* = x_{r4}^*, \ \bar{x}_{r4}^*(0) = x_{r4}^*(0) \\ s_{r4} = x_{r4} - \bar{x}_{r4}^* \\ \bar{v}_r = b_{r4}^{-1}[-\hat{d}_{r4} + \ddot{\bar{x}}_{r4}^* - k_{r4}s_{r4} - k_{r5}|s_{r4}|^{\lambda_{r4}}\,\mathrm{sgn}(s_{r4})] \end{cases} \tag{33}$$

where $0<\lambda_{r4}<1$, s_{r3} and s_{r4} are the error surfaces of the roll angle loop and roll angular rate loop, k_{r3} and k_{r4} are the corresponding error surface gains, τ_{r4} is the filter time constant.

3.4 Stability analysis

It is assumed that the estimated errors in the FTDO satisfy the following constraints [6]-[7]:

$$\begin{cases} |e_{p21}| < N_{p2}, |e_{p31}| < N_{p3}, |e_{p41}| < N_{p4} \\ |e_{y21}| < N_{y2}, |e_{y31}| < N_{y3}, |e_{y41}| < N_{y4} \\ |e_{r31}| < N_{r3}, |e_{r41}| < N_{r4} \end{cases} \tag{34}$$

where N_{pi}, N_{yi} and N_{ri} are positive constants, $i \in \{2,3,4\}$, $j \in \{3,4\}$.

Define the following filter errors:

$$\begin{cases} y_{p3} = \bar{x}_{p3}^* - x_{p3}^*, y_{p4} = \bar{x}_{p4}^* - x_{p4}^* \\ y_{y3} = \bar{x}_{y3}^* - x_{y3}^*, y_{y4} = \bar{x}_{y4}^* - x_{y4}^* \\ y_{r4} = \bar{x}_{r4}^* - x_{r4}^* \end{cases} \tag{35}$$

Then, the dynamics of the filter errors satisfy:

$$\begin{cases} \dot{y}_{p3} = -\tau_{p3}^{-1}y_{p3} - \dot{x}_{p3}^*, \dot{y}_{p4} = -\tau_{p4}^{-1}y_{p4} - \dot{x}_{p4}^* \\ \dot{y}_{y3} = -\tau_{y3}^{-1}y_{y3} - \dot{x}_{y3}^*, \dot{y}_{y4} = -\tau_{y4}^{-1}y_{y4} - \dot{x}_{y4}^* \\ \dot{y}_{r4} = -\tau_{r4}^{-1}y_{r4} - \dot{x}_{r4}^* \end{cases} \tag{36}$$

From equations (17)~(29) and (32)~(33), we can obtain:

$$\begin{cases} x_{p2} = -a_{p23}s_{p2} + x_{p2d} \\ x_{p3} = s_{p3} + \bar{x}_{p3}^* = s_{p3} + y_{p3} + x_{p3}^* \\ x_{p4} = s_{p4} + \bar{x}_{p4}^* = s_{p4} + y_{p4} + x_{p4}^* \\ \dot{s}_{p2} = -s_{p3} - y_{p3} - k_{p2}s_{p2} + \tilde{e}_{p21} \\ \dot{s}_{p3} = s_{p4} + y_{p4} - k_{p3}s_{p3} - e_{p31} \\ \dot{s}_{p4} = -k_{p4}s_{p4} - k_{p5}|s_{p4}|^{\lambda_{p4}}\,\mathrm{sgn}(s_{p4}) - e_{p41} \end{cases} \tag{37}$$

$$\begin{cases} x_{y2} = -a_{y23}s_{y2} + x_{y2d} \\ x_{y3} = s_{y3} + \bar{x}_{y3}^* = s_{y3} + y_{y3} + x_{y3}^* \\ x_{y4} = s_{y4} + \bar{x}_{y4}^* = s_{y4} + y_{y4} + x_{y4}^* \\ \dot{s}_{y2} = -s_{y3} - y_{y3} - k_{y2}s_{y2} - \tilde{e}_{y21} \\ \dot{s}_{y3} = s_{y4} + y_{y4} - k_{y3}s_{y3} - e_{y31} \\ \dot{s}_{y4} = -k_{y4}s_{y4} - k_{y5}|s_{y4}|^{\lambda_{y4}}\,\mathrm{sgn}(s_{y4}) - e_{y41} \end{cases} \tag{38}$$

$$\begin{cases} x_{r4} = s_{r4} + \bar{x}_{r4}^* = s_{r4} + y_{r4} + x_{r4}^* \\ \dot{s}_{r3} = s_{r4} + y_{r4} - k_{r3}s_{r3} - e_{r31} \\ \dot{s}_{r4} = -k_{r4}s_{r4} - k_{r5}|s_{r4}|^{\lambda_{r4}}\,\mathrm{sgn}(s_{r4}) - e_{r41} \end{cases} \tag{39}$$

where $\tilde{e}_{p21} = -\dfrac{m}{qSC_y^{\alpha}}e_{p21}$, $\tilde{e}_{y21} = \dfrac{m}{qSC_z^{\beta}}e_{y21}$. It is assumed that $|\tilde{e}_{p21}| \le \tilde{N}_{p2}$ and $|\tilde{e}_{y21}| < \tilde{N}_{y2}$.

For the system (9)~(11), consider the following Lyapunov function:

$$V = \tilde{V}_p + \tilde{V}_y + \tilde{V}_r \tag{40}$$

where

$$\tilde{V}_p = 0.5s_{p2}^2 + 0.5s_{p3}^2 + 0.5s_{p4}^2 + 0.5y_{p3}^2 + 0.5y_{p4}^2,$$

$$\tilde{V}_y = 0.5s_{y2}^2 + 0.5s_{y3}^2 + 0.5s_{y4}^2 + 0.5y_{y3}^2 + 0.5y_{y4}^2,$$

$$\tilde{V}_r = 0.5s_{r3}^2 + 0.5s_{r4}^2 + 0.5y_{r4}^2.$$

The coefficients and variables for the system (9) and their derivatives are all bounded. By some simple calculations, we have:

$$|\dot{x}_{p3}^*| \le \tilde{\eta}_{p3}(s_{p2}, s_{p3}, y_{p3}, e_{p21}, k_{p2}, x_{p2d}, \dot{x}_{p2d}, \ddot{x}_{p2d}) \tag{41}$$

$$|\dot{x}_{p4}^*| \le \tilde{\eta}_{p4}(s_{p2}, s_{p3}, s_{p4}, y_{p3}, y_{p4}, e_{p21}, e_{p31}, k_{p2}, k_{p3}, x_{p2d}, \dot{x}_{p2d}, \ddot{x}_{p2d}) \tag{42}$$

where $\tilde{\eta}_{p3}$ and $\tilde{\eta}_{p4}$ are both nonnegative continuous functions. For some given positive constants χ_p and R_p^*, the following sets

$$B_{p1} = \{[x_{p2d}, \dot{x}_{p2d}, \ddot{x}_{p2d}]^T, x_{p2d}^2 + \dot{x}_{p2d}^2 + \ddot{x}_{p2d}^2 \le \chi_p\} \tag{43}$$

$$B_{p2} = \{[s_{p2}, s_{p3}, s_{p4}, y_{p3}, y_{p4}, e_{p21}, e_{p31}]^T, \tilde{V}_p \le R_p^*\} \tag{44}$$

are compact. Obviously, $B_{p1}\times B_{p2}$ is also compact. Therefore, $\tilde{\eta}_{p3}$ and $\tilde{\eta}_{p4}$ have maximum values on the set $B_{p1}\times B_{p2}$, which satisfy the following conditions:

$$|\dot{x}_{p3}^*| \le M_{p3}, \ \ |\dot{x}_{p4}^*| \le M_{p4} \tag{45}$$

Based on the same method, we can also obtain:

$$|\dot{x}_{y3}^{*}| \le M_{y3}, \ |\dot{x}_{y4}^{*}| \le M_{y4}, \ |\dot{x}_{r4}^{*}| \le M_{r4} \tag{46}$$

where M_{p3}, M_{p4}, M_{y3}, M_{y4} and M_{r4} are positive constants.

From equation (37), we have:

$$\begin{aligned} s_{p2}\dot{s}_{p2} &= s_{p2}(-s_{p3} - y_{p3} - k_{p2}s_{p2} + \tilde{e}_{p21}) \\ &\le -k_{p2}s_{p2}^2 + 0.5(s_{p2}^2 + s_{p3}^2) + 0.5(s_{p2}^2 + y_{p3}^2) + 0.5(s_{p2}^2 + |\tilde{e}_{p21}|^2) \\ &\le (1.5 - k_{p2})s_{p2}^2 + 0.5s_{p3}^2 + 0.5y_{p3}^2 + 0.5\tilde{N}_{p2}^2 \end{aligned} \tag{47}$$

$$\begin{aligned} s_{p3}\dot{s}_{p3} &= s_{p3}(s_{p4} + y_{p4} - k_{p3}s_{p3} - e_{p31}) \\ &\le -k_{p3}s_{p3}^2 + 0.5(s_{p3}^2 + s_{p4}^2) + 0.5(s_{p3}^2 + y_{p4}^2) + 0.5(s_{p3}^2 + |e_{p31}|^2) \\ &\le (1.5 - k_{p3})s_{p3}^2 + 0.5s_{p4}^2 + 0.5y_{p4}^2 + 0.5N_{p3}^2 \end{aligned} \tag{48}$$

$$\begin{aligned} s_{p4}\dot{s}_{p4} &= s_{p4}[-k_{p4}s_{p4} - k_{p5}|s_{p4}|^{\lambda_{p4}}\,\mathrm{sgn}(s_{p4}) - e_{p41}] \\ &\le -k_{p4}s_{p4}^2 + 0.5(s_{p4}^2 + |e_{p41}|^2) - k_{p5}|s_{p4}|^{\lambda_{p4}+1} \\ &\le -k_{p4}s_{p4}^2 + 0.5(s_{p4}^2 + |e_{p41}|^2) + k_{p5}|s_{p4}|(1 + |s_{p4}|) \\ &\le -k_{p4}s_{p4}^2 + 0.5(s_{p4}^2 + |e_{p41}|^2) + k_{p5}(0.5 + 0.5s_{p4}^2 + s_{p4}^2) \\ &\le (0.5 - k_{p4} + 1.5k_{p5})s_{p4}^2 + 0.5N_{p4}^2 + 0.5k_{p5} \end{aligned} \tag{49}$$

$$y_{p3}\dot{y}_{p3} = y_{p3}(-\tau_{p3}^{-1}y_{p3} - \dot{x}_{p3}^{*}) \le -\tau_{p3}^{-1}y_{p3}^2 + 0.5(y_{p3}^2 + |\dot{x}_{p3}^{*}|^2) \le -\tau_{p3}^{-1}y_{p3}^2 + 0.5(y_{p3}^2 + M_{p3}^2) \tag{50}$$

$$y_{p4}\dot{y}_{p4} = y_{p4}(-\tau_{p4}^{-1}y_{p4} - \dot{x}_{p4}^{*}) \le -\tau_{p4}^{-1}y_{p4}^2 + 0.5(y_{p4}^2 + |\dot{x}_{p4}^{*}|^2) \le -\tau_{p4}^{-1}y_{p4}^2 + 0.5(y_{p4}^2 + M_{p4}^2) \tag{51}$$

Based on the same method, from equations (38) and (39), we can obtain:

$$\begin{cases} s_{y2}\dot{s}_{y2} \le (1.5 - k_{y2})s_{y2}^2 + 0.5s_{y3}^2 + 0.5y_{y3}^2 + 0.5\tilde{N}_{y2}^2 \\ s_{y3}\dot{s}_{y3} \le (1.5 - k_{y3})s_{y3}^2 + 0.5s_{y4}^2 + 0.5y_{y4}^2 + 0.5N_{y3}^2 \\ s_{y4}\dot{s}_{y4} \le (0.5 - k_{y4} + 1.5k_{y5})s_{y4}^2 + 0.5N_{y4}^2 + 0.5k_{y5} \\ y_{y3}\dot{y}_{y3} \le -\tau_{y3}^{-1}y_{y3}^2 + 0.5(y_{y3}^2 + M_{y3}^2) \\ y_{y4}\dot{y}_{y4} \le -\tau_{y4}^{-1}y_{y4}^2 + 0.5(y_{y4}^2 + M_{y4}^2) \end{cases} \tag{52}$$

$$\begin{cases} s_{r3}\dot{s}_{r3} \le (1.5 - k_{r3})s_{r3}^2 + 0.5s_{r4}^2 + 0.5y_{r4}^2 + 0.5N_{r3}^2 \\ s_{r4}\dot{s}_{r4} \le (0.5 - k_{r4} + 1.5k_{r5})s_{r4}^2 + 0.5N_{r4}^2 + 0.5k_{r5} \\ y_{r4}\dot{y}_{r4} \le -\tau_{r4}^{-1}y_{r4}^2 + 0.5(y_{r4}^2 + M_{r4}^2) \end{cases} \tag{53}$$

By taking the time derivative of $V(t)$ along the system (9)~(11), we have:

$$\begin{aligned} \dot{V} &= s_{p2}\dot{s}_{p2} + s_{p3}\dot{s}_{p3} + s_{p4}\dot{s}_{p4} + y_{p3}\dot{y}_{p3} + y_{p4}\dot{y}_{p4} + s_{y2}\dot{s}_{y2} \\ &\quad + s_{y3}\dot{s}_{y3} + s_{y4}\dot{s}_{y4} + y_{y3}\dot{y}_{y3} + y_{y4}\dot{y}_{y4} + s_{r3}\dot{s}_{r3} + s_{r4}\dot{s}_{r4} + y_{r4}\dot{y}_{r4} \\ &\le (1.5 - k_{p2})s_{p2}^2 + (2 - k_{p3})s_{p3}^2 + (1 - k_{p4} + 1.5k_{p5})s_{p4}^2 + (1 - \tau_{p3}^{-1})y_{p3}^2 \\ &\quad + (1 - \tau_{p4}^{-1})y_{p4}^2 + 0.5\tilde{N}_{p2}^2 + 0.5N_{p3}^2 + 0.5N_{p4}^2 + 0.5M_{p3}^2 + 0.5M_{p4}^2 + 0.5k_{p5} \\ &\quad + (1.5 - k_{y2})s_{y2}^2 + (2 - k_{y3})s_{y3}^2 + (1 - k_{y4} + 1.5k_{y5})s_{y4}^2 + (1 - \tau_{y3}^{-1})y_{y3}^2 \\ &\quad + (1 - \tau_{y4}^{-1})y_{y4}^2 + 0.5\tilde{N}_{y2}^2 + 0.5N_{y3}^2 + 0.5N_{y4}^2 + 0.5M_{y3}^2 + 0.5M_{y4}^2 + 0.5k_{y5} \\ &\quad + (1.5 - k_{r3})s_{r3}^2 + (1 - k_{r4} + 1.5k_{r5})s_{r4}^2 + (1 - \tau_{r4}^{-1})y_{r4}^2 + 0.5N_{r3}^2 + 0.5N_{r4}^2 + 0.5M_{r4}^2 + 0.5k_{r5} \end{aligned} \tag{54}$$

If the design parameters satisfy the following conditions:

$$\begin{cases} k_{p2} \ge 1.5 + 0.5\kappa, k_{p3} \ge 2 + 0.5\kappa, k_{p4} - 1.5k_{p5} \ge 1 + 0.5\kappa \\ \tau_{p3}^{-1} \ge 1 + 0.5\kappa, \tau_{p4}^{-1} \ge 1 + 0.5\kappa, k_{y2} \ge 1.5 + 0.5\kappa \\ k_{y3} \ge 2 + 0.5\kappa, k_{y4} - 1.5k_{y5} \ge 1 + 0.5\kappa \\ \tau_{y3}^{-1} \ge 1 + 0.5\kappa, \tau_{y4}^{-1} \ge 1 + 0.5\kappa, k_{r3} \ge 1.5 + 0.5\kappa \\ \tau_{r4}^{-1} \ge 1 + 0.5\kappa, k_{r4} - 1.5k_{r5} \ge 1 + 0.5\kappa \end{cases} \tag{55}$$

where κ is a positive real number, then we have:

$$\dot{V} \le -\kappa V + C \tag{56}$$

where

$$\begin{aligned} C &= 0.5\tilde{N}_{p2}^2 + 0.5N_{p3}^2 + 0.5N_{p4}^2 + 0.5M_{p3}^2 + 0.5M_{p4}^2 + 0.5k_{p5} + 0.5\tilde{N}_{y2}^2 + 0.5N_{y3}^2 \\ &\quad + 0.5N_{y4}^2 + 0.5M_{y3}^2 + 0.5M_{y4}^2 + 0.5k_{y5} + 0.5N_{r3}^2 + 0.5N_{r4}^2 + 0.5M_{r4}^2 + 0.5k_{r5}. \end{aligned}$$

Based on the comparison principle, from equation (56) we can obtain:

$$V(t) \le \frac{[\kappa V(0) - C]e^{-\kappa t} + C}{\kappa} \tag{57}$$

If the parameter κ is selected large enough, the parameter C/κ can be made arbitrarily small. Therefore, the error surfaces and filter errors are all uniformly ultimately bounded, and we can obtain the small miss distance.

3.5 Robust least-squares weighted control allocation

In this section, we proposed a novel RLSWCA algorithm to distribute the virtual control command among the individual actuators (aerodynamic fins and reaction jets), while also taking into account the uncertainty in the control effectiveness matrix.

The elements of the uncertain terms $\triangle B_e$ are all usually small bounded. Therefore, we assume that the uncertainty in the control effectiveness matrix satisfies the following constraint:

$$||\Delta \boldsymbol{B}_e||_{\infty} \le \eta \tag{58}$$

where η is known constant. Generally, the individual actuators constraints are given as follows:

$$\begin{cases} \underline{\boldsymbol{u}}(t) \le \boldsymbol{u}(t) \le \overline{\boldsymbol{u}}(t), \underline{\dot{\boldsymbol{u}}} \le \dot{\boldsymbol{u}}(t) \le \overline{\dot{\boldsymbol{u}}} \\ \underline{\boldsymbol{u}}(t) = \max\{\boldsymbol{u}_{\min}, \boldsymbol{u}(t-T_s) + \underline{\dot{\boldsymbol{u}}} T_s\} \\ \overline{\boldsymbol{u}}(t) = \min\{\boldsymbol{u}_{\max}, \boldsymbol{u}(t-T_s) + \overline{\dot{\boldsymbol{u}}} T_s\} \end{cases} \tag{59}$$

where T_s is the sampling time.

The following transformation is introduced to avoid the uneven distribution problem:

$$\tilde{\boldsymbol{u}} = \boldsymbol{W}_u^{-1} \boldsymbol{u} \tag{60}$$

where W_u>0 is the transformation matrix.

For the control allocation problem (8) and (58)~(60), we can obtain the optimal input $\tilde{\boldsymbol{u}}$ based on the robust least-squares method in [22] and [23]:

$$\tilde{\boldsymbol{u}} = \arg \min_{\boldsymbol{W}_u^{-1}\underline{\boldsymbol{u}}(t) \le \tilde{\boldsymbol{u}}(t) \le \boldsymbol{W}_u^{-1}\overline{\boldsymbol{u}}(t)} \max_{\|\Delta \boldsymbol{B}_c\|_\infty \le \eta} J_c \tag{61}$$

where $J_c = \|(\boldsymbol{B}_c + \Delta \boldsymbol{B}_c)\boldsymbol{W}_u \tilde{\boldsymbol{u}} - \boldsymbol{v}\|$. Furthermore, we can obtain the following worst-case residual:

$$\chi(\tilde{\boldsymbol{u}}) = \max_{\|\Delta \boldsymbol{B}_c\|_\infty \le \eta} \|(\boldsymbol{B}_c + \Delta \boldsymbol{B}_c)\boldsymbol{W}_u \tilde{\boldsymbol{u}} - \boldsymbol{v}\| \tag{62}$$

Based on the triangle inequality, we have

$$\begin{aligned} \chi(\tilde{\boldsymbol{u}}) &\le \max_{\|\Delta \boldsymbol{B}_c\|_\infty \le \eta} (\|\boldsymbol{B}_c \boldsymbol{W}_u \tilde{\boldsymbol{u}} - \boldsymbol{v}\| + \|\Delta \boldsymbol{B}_c \boldsymbol{W}_u \tilde{\boldsymbol{u}}\|) \\ &= \|\boldsymbol{B}_c \boldsymbol{W}_u \tilde{\boldsymbol{u}} - \boldsymbol{v}\| + \max_{\|\Delta \boldsymbol{B}_c\|_\infty \le \eta} \|\Delta \boldsymbol{B}_c \boldsymbol{W}_u \tilde{\boldsymbol{u}}\| \end{aligned} \tag{63}$$

Assume that

$$\Delta \boldsymbol{B}_c \boldsymbol{W}_u = \eta \frac{\boldsymbol{\varepsilon}_c \tilde{\boldsymbol{u}}^T}{\|\tilde{\boldsymbol{u}}\|} \tag{64}$$

where $\boldsymbol{\varepsilon}_c = \begin{cases} \frac{\boldsymbol{B}_c \boldsymbol{W}_u \tilde{\boldsymbol{u}} - \boldsymbol{v}}{\|\boldsymbol{B}_c \boldsymbol{W}_u \tilde{\boldsymbol{u}} - \boldsymbol{v}\|}, & \text{if } \boldsymbol{B}_c \boldsymbol{W}_u \tilde{\boldsymbol{u}} \ne \boldsymbol{v} \\ \text{any unit norm vector, otherwise} \end{cases}$.

Then, in the direction of ε_c, the worst-case residual is:

$$\chi(\tilde{\boldsymbol{u}}) = \|\boldsymbol{B}_c \boldsymbol{W}_u \tilde{\boldsymbol{u}} - \boldsymbol{v}\| + \eta \|\tilde{\boldsymbol{u}}\| \tag{65}$$

To this end, the worst-case residual (65) also satisfies the following constraint:

$$\|\boldsymbol{B}_c \boldsymbol{W}_u \tilde{\boldsymbol{u}} - \boldsymbol{v}\| + \eta \|\tilde{\boldsymbol{u}}\| \le \lambda_e \tag{66}$$

where λ_e is the upper bound of the residual to be minimized.

Based on the method [23], the RLSWCA problem can be rewritten as a second order cone program (SOCP) problem:

$$\min_{\tilde{\boldsymbol{u}}, \tau_e, \lambda_e} \lambda_e \tag{67}$$

subject to $\|\boldsymbol{B}_c \boldsymbol{W}_u \tilde{\boldsymbol{u}} - \boldsymbol{v}\| \le \lambda_e - \tau_e$, $\eta \|\tilde{\boldsymbol{u}}\| \le \tau_e$ and $\boldsymbol{W}_u^{-1}\underline{\boldsymbol{u}}(t) \le \tilde{\boldsymbol{u}}(t) \le \boldsymbol{W}_u^{-1}\overline{\boldsymbol{u}}(t)$.

Then, the optimal solution u of the RLSWCA problem can be given by:

$$\boldsymbol{u} = \begin{cases} \boldsymbol{W}_u (\mu \boldsymbol{I} + \boldsymbol{W}_u \boldsymbol{B}_c^T \boldsymbol{B}_c \boldsymbol{W}_u)^{-1} \boldsymbol{W}_u \boldsymbol{B}_c^T \boldsymbol{v} & \text{if } \mu > 0 \\ \boldsymbol{W}_u (\boldsymbol{W}_u \boldsymbol{B}_c^T \boldsymbol{B}_c \boldsymbol{W}_u)^{-1} \boldsymbol{W}_u \boldsymbol{B}_c^T \boldsymbol{v} & \text{else} \end{cases} \tag{68}$$

where $\mu = (\lambda_e - \tau_e)\tau_e \eta^2 / (\tau_e^2 + \eta^2 \tilde{s}) \ge 0, \tilde{s} = \|\boldsymbol{W}_u^{-1}\overline{\boldsymbol{u}}\|^2 + \|\boldsymbol{W}_u^{-1}\underline{\boldsymbol{u}}\|^2$, λ_e and τ_e are the optimal solutions of the minimization problem (67). The proof procedure can be easily obtained from [23].

Based on the above analysis, the structure diagram of a three-channel independent IGC system for the NSI is shown in Fig. 2.

4. Simulation results

Some simulation results are presented to illustrate the effectiveness of the proposed three-channel independent IGC algorithm and RLSWCA scheme.

The parameters of the FTDOs (13)~(16) and (31) are selected as follows:

$\lambda_{p20} = 20$, $\lambda_{p30} = \lambda_{p40} = 2$, $\lambda_{pi1} = 1.5$, $\lambda_{pi2} = 1.1$, $q_{pi} = 0.5$, $p_{pi} = 8$, $i \in \{2, 3, 4\}$;

$\lambda_{y20} = 20$, $\lambda_{y30} = \lambda_{y40} = 2$, $\lambda_{yi1} = 1.5$, $\lambda_{yi2} = 1.1$, $q_{yi} = 0.5$, $p_{yi} = 8$, $i \in \{2, 3, 4\}$;

$\lambda_{ri0} = 2$, $\lambda_{ri1} = 1.5$, $\lambda_{ri2} = 1.1$, $q_{ri} = 0.5$, $p_{ri} = 8$, $i \in \{3, 4\}$;

$L_{p2} = L_{y2} = L_{r3} = 100$, $L_{p3} = L_{y3} = 10$, $L_{p4} = L_{y4} = L_{r4} = 50$.

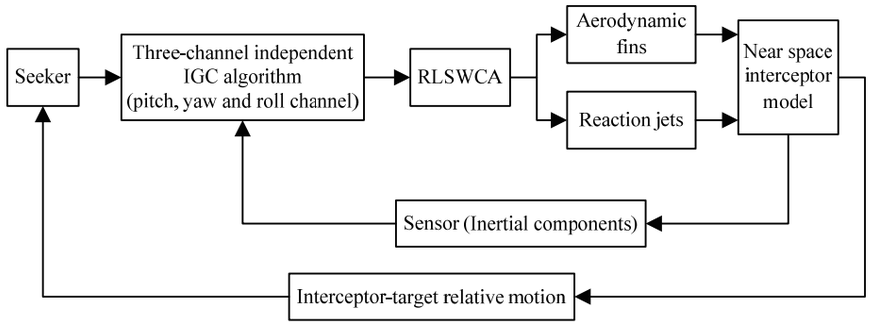

Fig. 2. Structure diagram of a three-channel independent IGC system

The parameters of the proposed three-channel independent IGC algorithm (17)~(29) and (32)-(33) are selected as follows:

$$k_{p2}=k_{y2}=2.5,\ k_{p3}=k_{y3}=k_{r3}=10,\ k_{p4}=k_{y4}=k_{r4}=40,$$

$$k_{p5}=k_{y5}=k_{r5}=5,\ \tau_{p3}=\tau_{y3}=0.1,\ \tau_{p4}=\tau_{y4}=\tau_{r4}=0.025,$$

$$\lambda_{p4}=\lambda_{y4}=\lambda_{r4}=0.6,\ x_{p2d}=x_{y2d}=x_{r3d}=0.$$

The proposed three-channel independent IGC algorithm incorporating the RLSWCA method (denoted by IGC+FTDO+RLSWCA) is firstly applied to the NSI guidance and control system. Furthermore, we also studied the proportional navigation guidance (PNG) law and sliding mode guidance (SMG) law combined with the traditional backstepping sliding mode control law and RLSWCA method (denoted by PNG+BSM+RLSWCA and SMG+BSM+RLSWCA, respectively) for the simulation comparison. This was in line with traditional guidance and control separation design. The PNG law and SMG law are given as follows:

$$a_{m4\varepsilon}=-N_p\dot{r}\dot{q}_\varepsilon,\ a_{m4\beta}=N_p\dot{r}\dot{q}_\beta \tag{69}$$

$$a_{m4\varepsilon}=-N_s\dot{r}\dot{q}_\varepsilon+\bar{\varepsilon}\,\mathrm{sgn}(\dot{q}_\varepsilon),\ a_{m4\beta}=N_s\dot{r}\dot{q}_\beta-\bar{\varepsilon}\,\mathrm{sgn}(\dot{q}_\beta) \tag{70}$$

where $N_p=3.2$, $N_s=4.5$ and $\bar{\varepsilon}=200$.

In this paper, we select the following six interception conditions to illustrate the effectiveness of the above three guidance and control schemes:

Case 1 and Case 4: No maneuvering target, $a_{tc}=a_{t\beta}=0\mathrm{m/s^2}$;

Case 2 and Case 5: Step maneuvering target, $a_{tc}=a_{t\beta}=40\mathrm{m/s^2}$;

Case 3 and Case 6: Sinusoidal maneuvering target, $a_{tc}=a_{t\beta}=40\sin(t)\mathrm{m/s^2}$.

The initial conditions for Cases 1~3 are give as follows: The initial positions of the interceptor are $x_{m0}=y_{m0}=z_{m0}=0$m; the velocities of the interceptor and target are $V_{m0}=1500$m/s and $V_{t0}=1700$m/s, respectively; the initial flight-path angle and heading angle of the interceptor and target are $\theta_{m0}=26^o$, $\psi_{vm0}=-5^o$, $\theta_{t0}=-10^o$ and $\psi_{vt0}=120^o$; the initial relative distance is $r_0=1.8\times10^4$; the azimuth angle and elevation angle are $q_{\varepsilon0}=20^o$ and $q_{\beta0}=-36^o$, respectively. The initial conditions for Cases 4~6 are also give as follows: The initial positions of the target are $x_{t0}=15204.5$m, $t_{t0}=6840.4$m and $z_{t0}=11046.7$m; the other conditions are the same as Cases 1~3.

In the simulation process, we select the external disturbance of the control system loop as $d_r=d_\beta=d_\alpha=0.2\sin(t)$ and $d_{\omega_x}=d_{\omega_y}=d_{\omega_z}=\sin(t)$, respectively.

Figure 3 shows the response curves of the LOS angular rate for Case 1 based on the above three guidance and control schemes, and we can see that the proposed three-channel independent IGC algorithm can make the LOS angular rate converge to the steady state value more quickly; i.e., the small miss distance can be obtained. Fig. 4 and Fig. 6 show the curves of the interceptor attitude and control inputs. The actual and estimated value responses of the target acceleration are shown in Fig. 5, and we can observe that the proposed FTDO can provide a satisfactory estimation of performance. The simulation curves for Case 2 and Case 3 are shown in Figs. 7~14, the simulation curves for Case 4~6 and the analysis processes are similar, which are omitted here for brevity.

Define the control energy function as follows: $J_u=0.5\int_0^t\|\boldsymbol{B}_c\boldsymbol{u}\|^2dt$. Table 1 shows the miss distances, interception time and control energy of the three guidance and control schemes for Cases 1~6. The proposed IGC

Table 1. Simulation results of the three guidance and control schemes

Case	Design method	Miss distance	Interception time	Control energy
1	PNG+BSM+RLSWCA	0.4139 m	6.318 s	1.361×10^6
	SMG+BSM+RLSWCA	0.2652 m	6.318 s	2.268×10^6
	IGC+FTDO+RLSWCA	0.1282 m	6.318 s	2.513×10^7
2	PNG+BSM+RLSWCA	1.2580 m	6.321 s	3.216×10^7
	SMG+BSM+RLSWCA	1.0120 m	6.319 s	2.582×10^7
	IGC+FTDO+RLSWCA	0.1928 m	6.318 s	4.069×10^7
3	PNG+BSM+RLSWCA	1.2360 m	6.320 s	2.848×10^7
	SMG+BSM+RLSWCA	1.1970 m	6.318 s	1.347×10^7
	IGC+FTDO+RLSWCA	0.2110 m	6.318 s	3.755×10^7
4	PNG+BSM+RLSWCA	0.4640 m	7.020 s	1.195×10^6
	SMG+BSM+RLSWCA	0.2948 m	7.020 s	1.902×10^6
	IGC+FTDO+RLSWCA	0.1344 m	7.020 s	2.468×10^7
5	PNG+BSM+RLSWCA	1.1140 m	7.023 s	3.496×10^7
	SMG+BSM+RLSWCA	0.9619 m	7.022 s	2.283×10^7
	IGC+FTDO+RLSWCA	0.1968 m	7.020 s	4.375×10^7
6	PNG+BSM+RLSWCA	0.9931 m	7.022 s	1.180×10^7
	SMG+BSM+RLSWCA	1.3220 m	7.021 s	1.260×10^7
	IGC+FTDO+RLSWCA	0.1481 m	7.020 s	4.235×10^7

DOI: http://dx.doi.org/10.5139/IJASS.2015.16.2.278

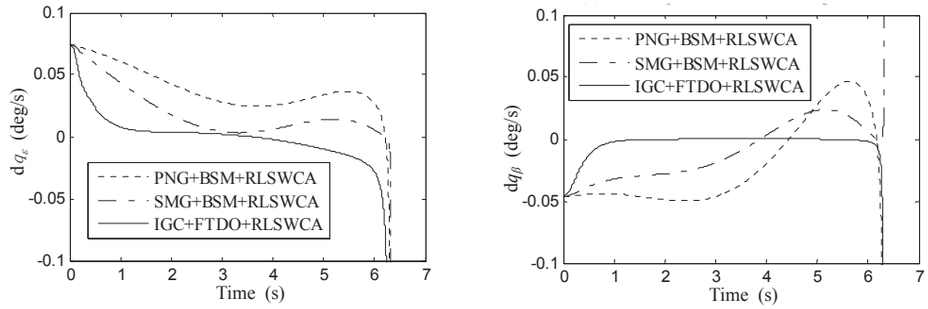

(a) LOS angular rate in vertical plane (b) LOS angular rate in lateral plan

Fig. 3. Trajectories of the LOS angular rate for Case 1

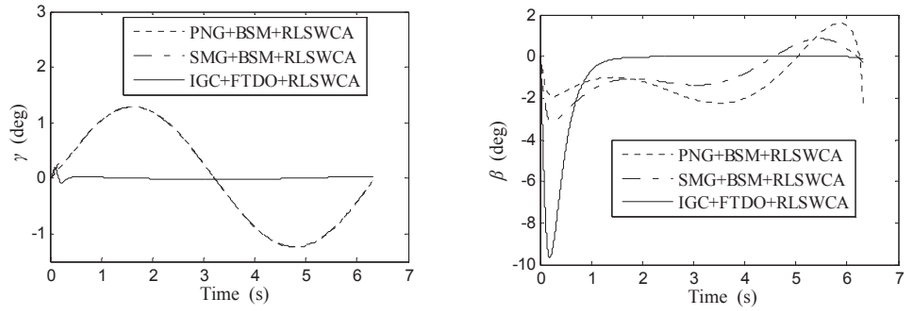

(a) Roll angle (b) Sideslip angle

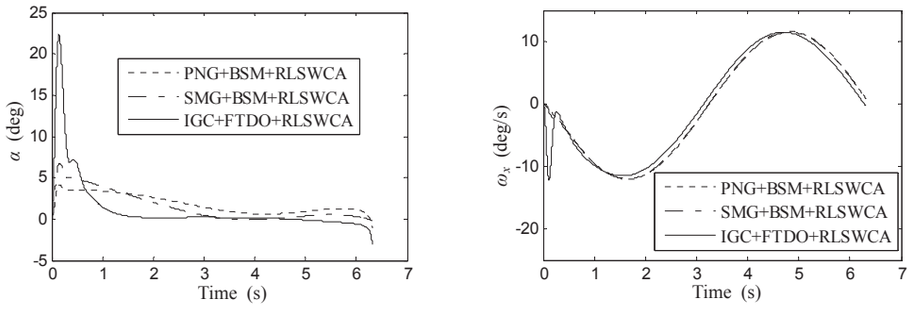

(c) Angle of attack (d) Roll rate

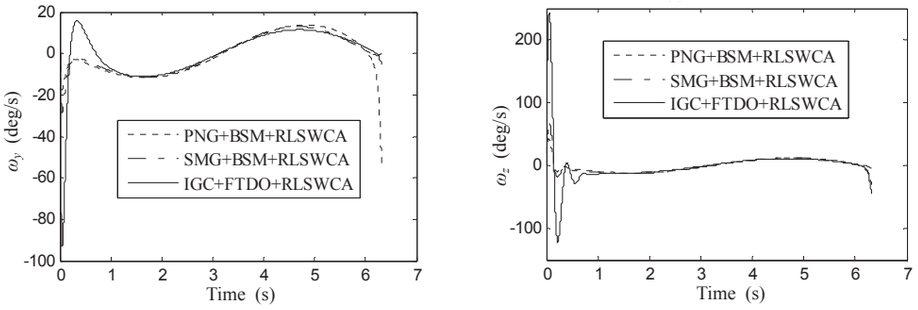

(e) Yaw rate (f) Pitch rate

Fig. 4. Trajectories of the angle and angular rate for Case 1

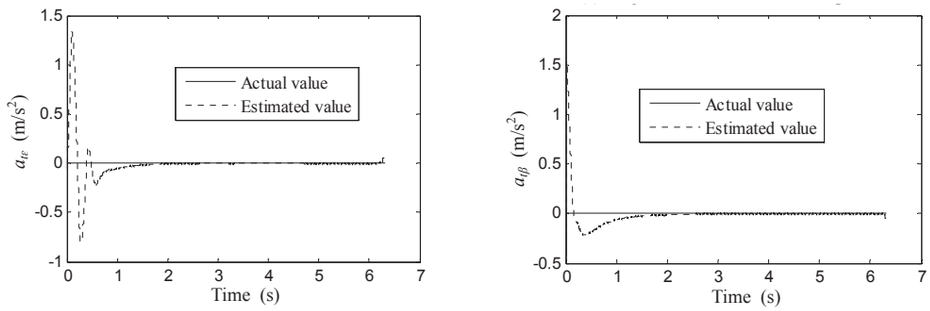

(a) Target acceleration in vertical plane (b) Target acceleration in lateral plane

Fig. 5. Actual and estimated values of target acceleration for Case 1

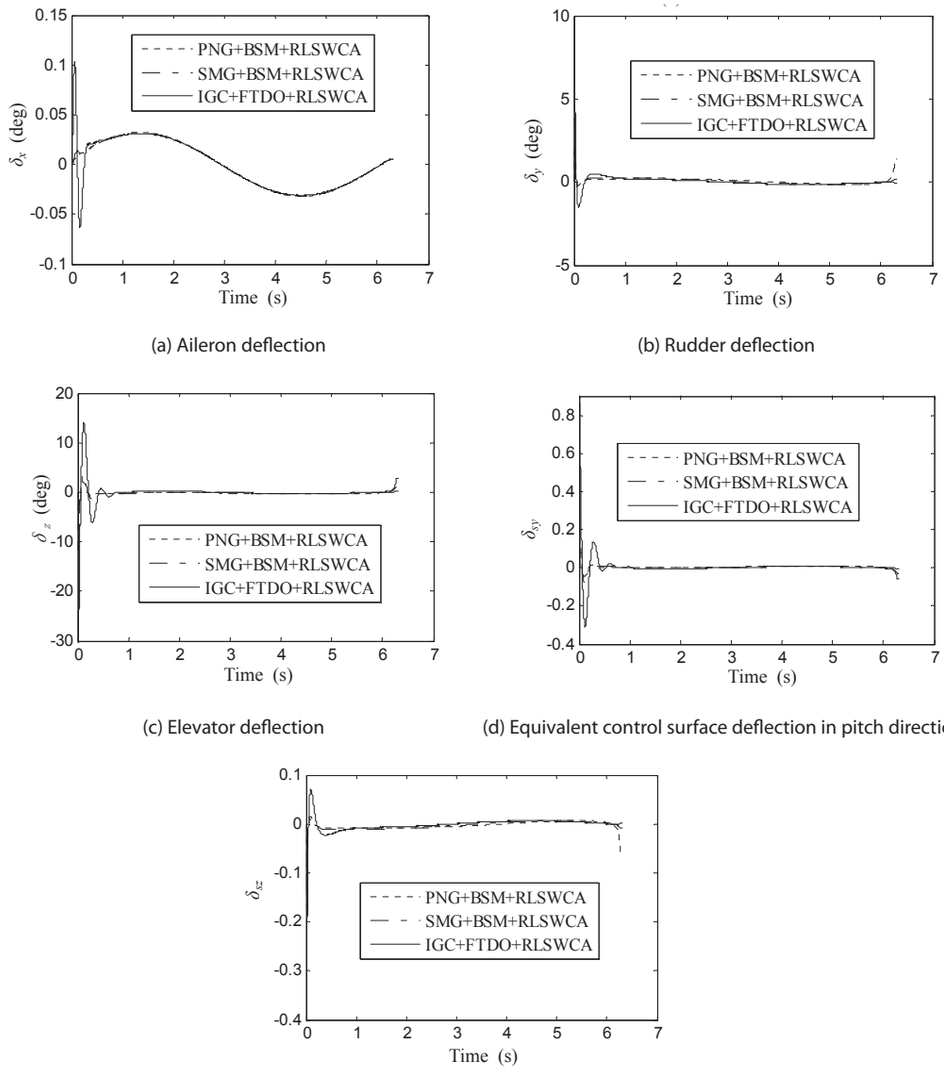

(a) Aileron deflection (b) Rudder deflection

(c) Elevator deflection (d) Equivalent control surface deflection in pitch direction

(e) Equivalent control surface deflection in yaw direction

Fig. 6. Trajectories of the actual control inputs for Case 1

DOI: http://dx.doi.org/10.5139/IJASS.2015.16.2.278

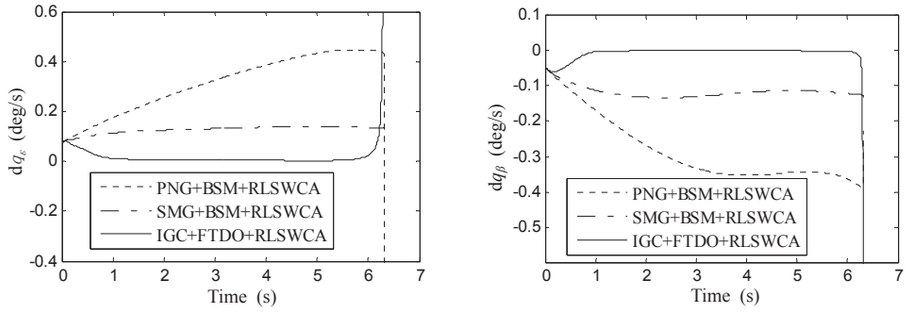

(a) LOS angular rate in vertical plane (b) LOS angular rate in lateral plane

Fig. 7. Trajectories of the LOS angular rate for Case 2

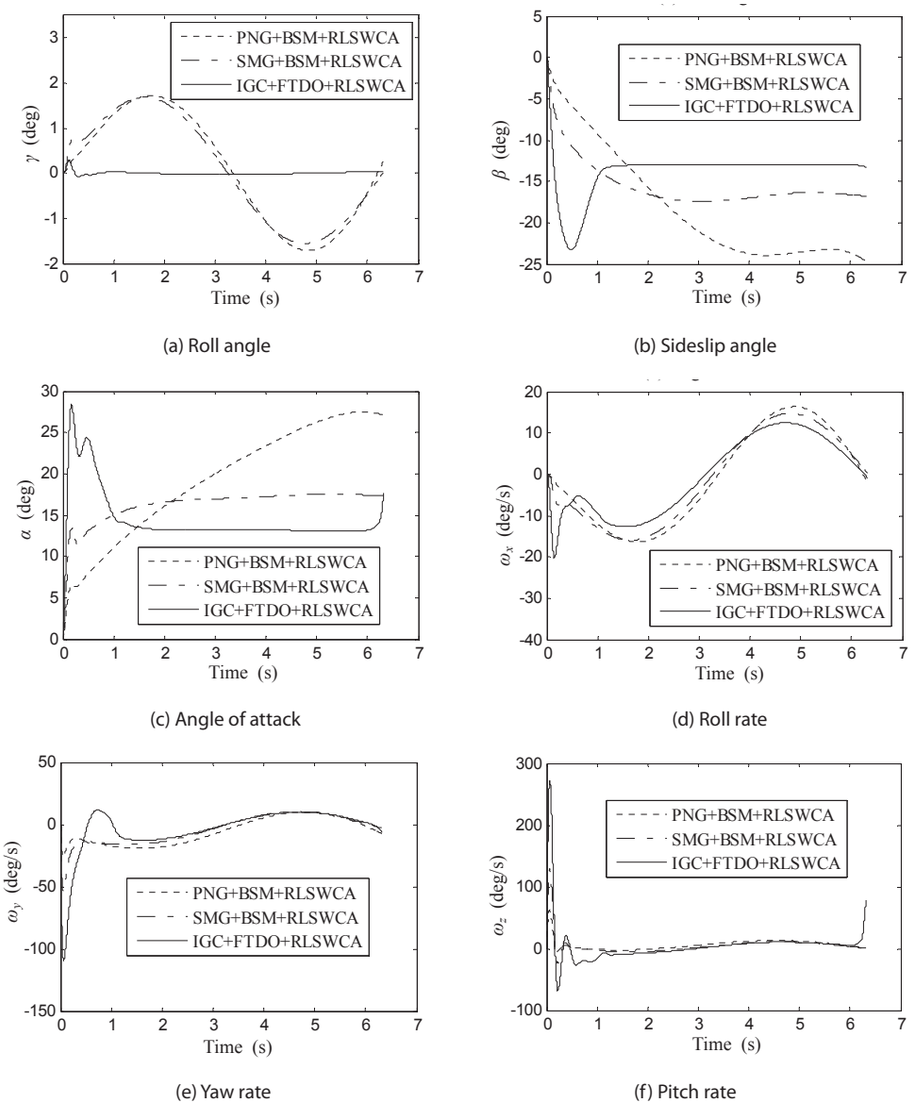

(a) Roll angle (b) Sideslip angle

(c) Angle of attack (d) Roll rate

(e) Yaw rate (f) Pitch rate

Fig. 8. Trajectories of the angle and angular rate for Case 2

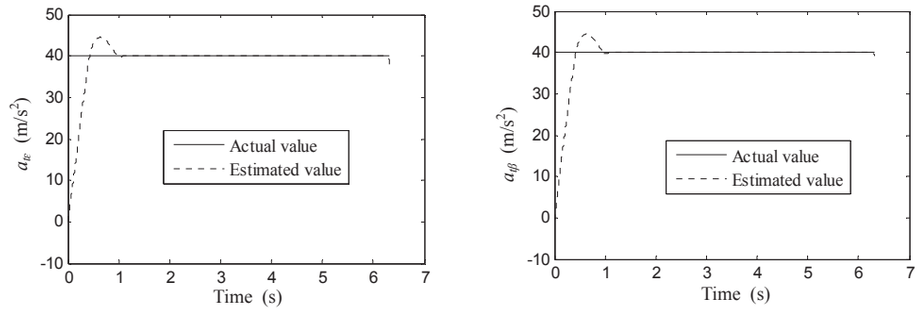

(a) Target acceleration in vertical plane (b) Target acceleration in lateral plane

Fig. 9. Actual and estimated values of target acceleration for Case 2

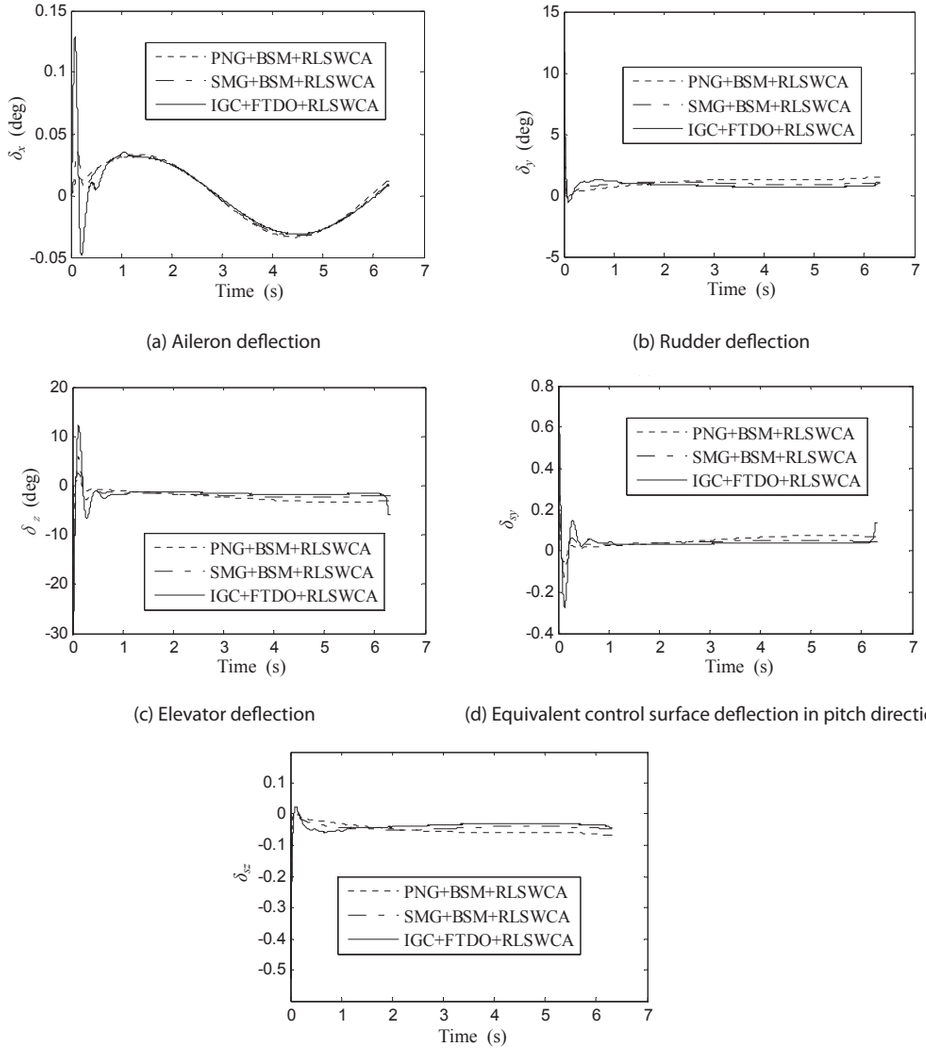

(a) Aileron deflection (b) Rudder deflection

(c) Elevator deflection (d) Equivalent control surface deflection in pitch direction

(e) Equivalent control surface deflection in yaw direction

Fig. 10. Trajectories of the actual control inputs for Case 2

DOI: http://dx.doi.org/10.5139/IJASS.2015.16.2.278

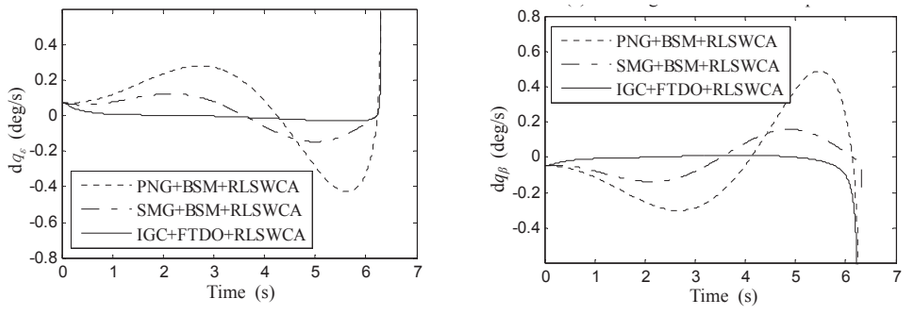

(a) LOS angular rate in vertical plane (b) LOS angular rate in lateral plane

Fig. 11. Trajectories of the LOS angular rate for Case 3

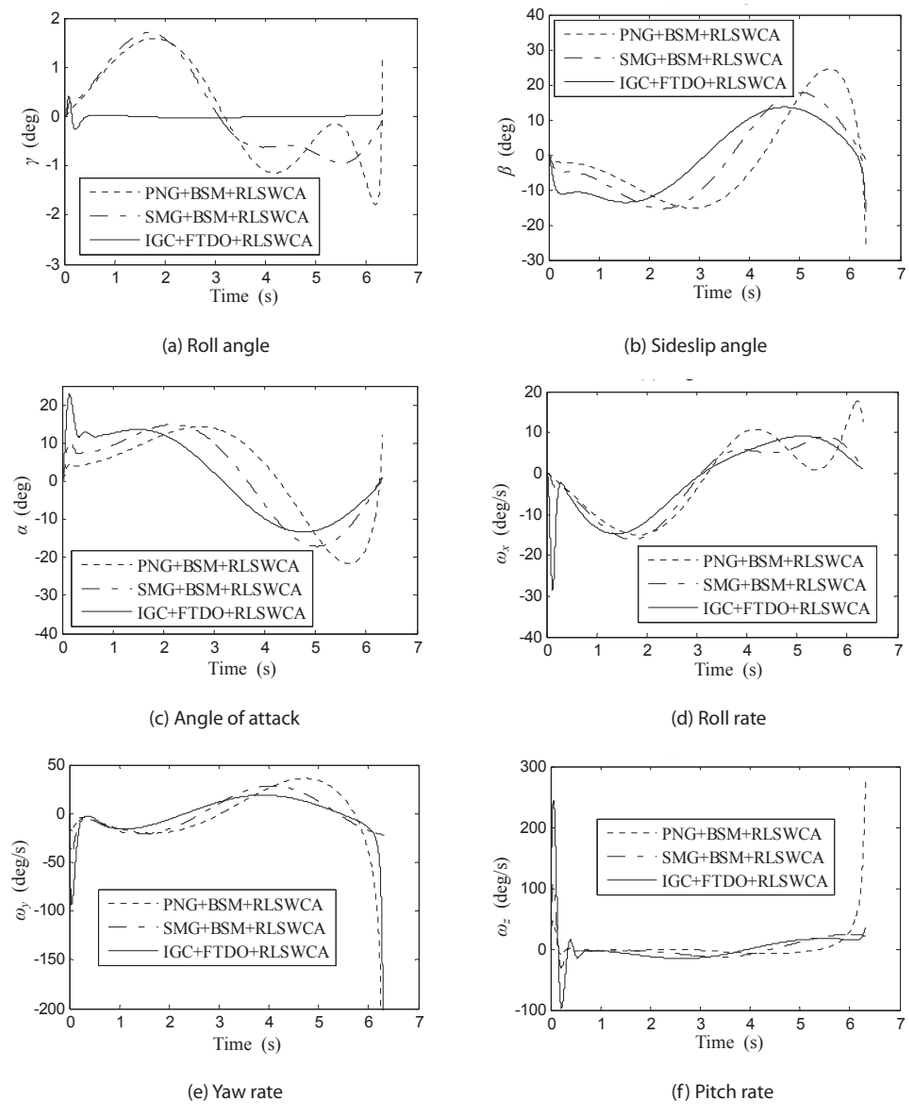

(a) Roll angle (b) Sideslip angle

(c) Angle of attack (d) Roll rate

(e) Yaw rate (f) Pitch rate

Fig. 12. Trajectories of the angle and angular rate for Case 3

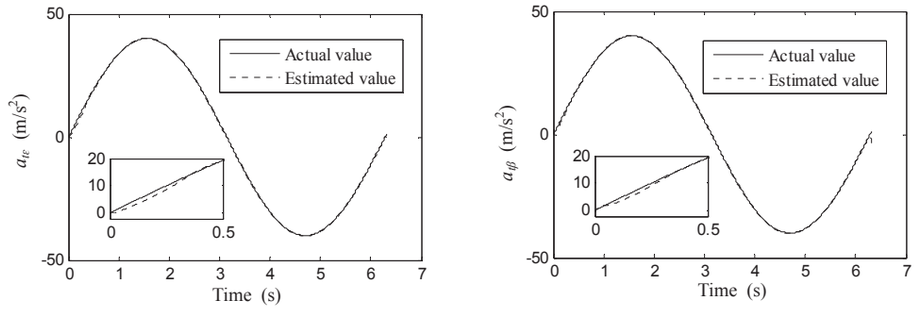

(a) Target acceleration in vertical plane (b) Target acceleration in lateral plane

Fig 13. Actual and estimated values of target acceleration for Case 2

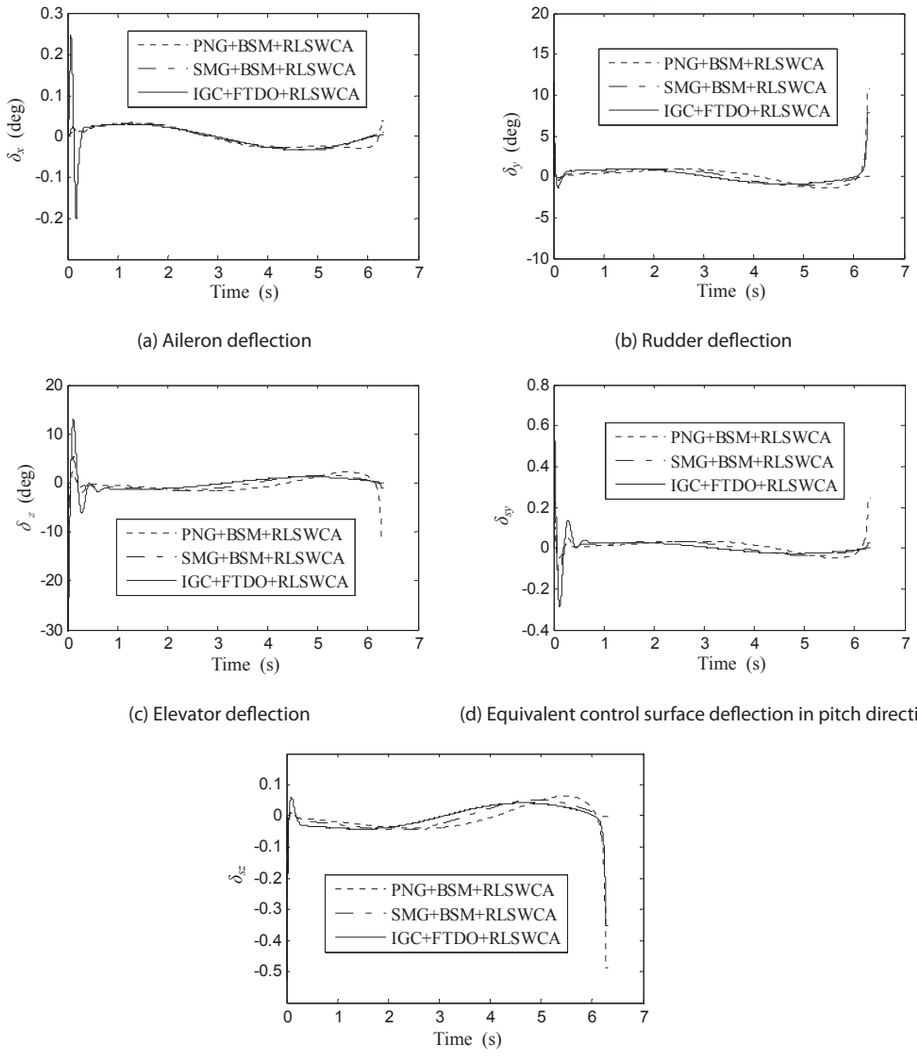

(a) Aileron deflection (b) Rudder deflection

(c) Elevator deflection (d) Equivalent control surface deflection in pitch direction

(e) Equivalent control surface deflection in yaw direction

Fig. 14. Trajectories of the actual control inputs for Case 2

DOI: http://dx.doi.org/10.5139/IJASS.2015.16.2.278

algorithm required more control energy to obtain the small miss distance. Compared with PNG+BSM+RLSWCA and SMG+BSM+RLSWCA, it can be observed from Table 1 that the miss distance and interception time for the proposed IGC algorithm are minimal, since this method considers the effects of the target maneuver and external distance in the control system loop, and the couplings between the guidance loop and control loop.

Remark 1. In general, the knowledge and experience of experts (including control engineers and operators) are employed to determine the design parameters. For the design parameters of the pitch channel, the FTDO parameters are often selected as λ_{p20}=20, λ_{p30}=λ_{p40}=2, λ_{pi1}=1.5, λ_{pi2}=1.1, q_{pi}=0.5 and p_{pi}=8, $i\in\{2, 3, 4\}$; the filter time constants are often selected as $\tau_{p3}\in\{0.01, 0.2\}$ and $\tau_{p4}\in\{0.01, 0.2\}$, and then the controller parameters are often selected as $k_{p2}\in\{2, 5\}$, $k_{p3}=1/\tau_{p3}$, $k_{p4}=1/\tau_{p4}$, $k_{p5}\in\{1, 10\}$ and $\lambda_{p4}\in(0, 1)$. The design parameters of the yaw channel and roll channel are similar.

5. Conclusion

In this paper, a novel three-channel independent IGC design method is proposed for the NSI, based on the backstepping sliding mode and FTDO, which also take into account the couplings of the guidance and control system and those between the different channels of interceptor. In the proposed method, the FTDO is firstly constructed to estimate the target acceleration and the disturbance of the control system loop, and the IGC algorithm based on the backstepping sliding mode is given to obtain the desired control moment. Moreover, the stability analysis based on the Lyapunov theory shows that the proposed IGC scheme can make the LOS angular rate to converge into a small neighborhood of zero. Finally, simulation results also illustrate the effectiveness of the proposed IGC algorithm.

References

[1] Hou, M., Liang, X. and Duan, G., "Adaptive block dynamic surface control for integrated missile guidance and autopilot", *Chinese Journal of Aeronautics*, Vol. 26, No. 3, 2013, pp. 741-750.

[2] Ran, M., Wang, Q. and Hou, D., et al., "Backstepping design of missile guidance and control based on adaptive fuzzy sliding mode control", *Chinese Journal of Aeronautics*, Vol. 27, No. 3, 2014, pp. 634-642.

[3] Menon, P. and Ohlmeyer, E., "Integrated design of agile missile guidance and autopilot systems", *Control Engineering Practice*, Vol. 9, No. 10, 2001, pp. 1095-1106.

[4] Menon, P., Sweriduk, G. and Ohlmeyer, E., et al., "Integrated guidance and control of moving-mass actuated kinetic warheads", *AIAA Journal of Guidance, Control and Dynamics*, Vol. 27, No. 1, 2004, pp. 118-126.

[5] Xue, W., Huang, C. and Huang, Y., "Design methods for the integrated guidance and control system", *Control Theory & Applications*, Vol. 30, No. 12, 2013, pp. 1511-1520. [in Chinese]

[6] Shtessel, Y. and Tournes, C., "Integrated higher-order sliding mode guidance and autopilot for dual control missiles", *AIAA Journal of Guidance, Control and Dynamics*, Vol. 32, No. 1, 2009, pp. 79-94.

[7] Shtessel, Y., Shkolnikov, I. and Levant, A., "Guidance and control of missile interceptor using second-order sliding modes", *IEEE Transactions on Aerospace and Electronic Systems*, Vol. 45, No. 1, 2009, pp. 110-124.

[8] Dong, F., Lei, H. and Zhou, C., et al., "Research of integrated robust high order sliding mode guidance and control for missiles", *Acta Aeronautica et Astronautica Sinica*, Vol. 34, No. 9, 2013, pp. 2212-2218. [in Chinese]

[9] Vaddi, S., Menon, P. and Ohlmeyer, E., "Numerical state-dependent Riccati equation approach for missile integrated guidance control", *AIAA Journal of Guidance, Control and Dynamics*, Vol. 32, No. 2, 2009, pp. 699-703.

[10] Xin, M., Balakrishnan, S. and Ohlmeyer, E., "Integrated guidance and control of missiles with θ-D method", *IEEE Transactions on Control Systems Technology*, Vol. 14, No. 6, 2006, pp. 981-992.

[11] Yan, H. and Ji, H., "Integrated guidance and control for dual-control missiles based on small-gain theorem", *Automatica*, Vol. 48, No. 10, 2012, pp. 2686-2692.

[12] Wang, X. and Wang, J., "Partial integrated missile guidance and control with finite time convergence", *AIAA Journal of Guidance, Control and Dynamics*, Vol. 36, No. 5, 2013, pp. 1399 -1409.

[13] Wang, X. and Wang, J., "Partial integrated guidance and control for missiles with three-dimensional impact angle constraints", *AIAA Journal of Guidance, Control and Dynamics*, Vol. 37, No. 2, 2014, pp. 644-657.

[14] Chen, W., "Disturbance observer based control for nonlinear systems", *IEEE/ASME Transactions on Mechatronics*, Vol. 9, No. 4, 2004, pp. 706-710.

[15] Wei, X. and Guo, L., "Composite disturbance-observer-based control and H_∞ control for complex continuous models", *International Journal of Robust and Nonlinear Control*, Vol. 20, No. 1, 2004, pp. 106-118.

[16] Yang, J., Su, J. and Li, S., et al., "High-order mismatched disturbance compensation for motion control systems via a continuous dynamic sliding-mode approach", *IEEE*

Transactions on Industrial Informatics, Vol. 10, No. 1, 2014, pp. 604-614.

[17] Chen, W., "Nonlinear disturbance observer-enhanced dynamic inversion control of missiles", *AIAA Journal of Guidance, Control, and Dynamics*, Vol. 26, No. 1, 2003, pp. 161-166.

[18] Li, S. and Yang, J., "Robust autopilot design for bank-to-turn missiles using disturbance observers", *IEEE Transactions on Aerospace and Electronic Systems*, Vol. 49, No. 1, 2013, pp. 558-579.

[19] Yang, J., Li, S. and Sun, C., "Nonlinear-disturbance-observer-based robust flight control for airbreathing hypersonic vehicles", *IEEE Transactions on Aerospace and Electronic Systems*, Vol. 49, No. 2, 2013, pp. 1263-1275.

[20] Shtessel, Y., Shkolnikov, I. and Levant, A., "Smooth second-order sliding modes: missile guidance application", *Automatica*, Vol. 43, No. 8, 2007, pp. 1470-1476.

[21] Johansen, T. and Fossen, T., "Control allocation--a survey", *Automatica*, Vol. 49, No. 5, 2013, pp. 1087-1103.

[22] Ghaoui, L. and Lebret, H., "Robust solutions to least squares problems with uncertain data", *SIAM Journal on Matrix Analysis and Applications*, Vol. 18, No. 4, 1997, pp. 1035-1064.

[23] Cui, L. and Yang, Y., "Disturbance rejection and robust least-squares control allocation in flight control system", *AIAA Journal of Guidance, Control, and Dynamics*, Vol. 34, No. 6, 2011, pp. 1632-1643.

[24] Zhou, D., Sun, S. and Teo, K., "Guidance laws with finite time convergence", *AIAA Journal of Guidance, Control, and Dynamics*, Vol. 32, No. 6, 2009, pp. 1838-1846.

[25] Zhou, D. and Shao, C., "Dynamics and autopilot design for endoatmospheric interceptors with dual control systems", *Aerospace Science and Technology*, Vol. 13, No. 6, 2009, pp. 291-300.

DOI: http://dx.doi.org/10.5139/IJASS.2015.16.2.278